Scientia Iranica A (2022) 29(6), 2953–2967

Sharif University of Technology
Scientia Iranica
Transactions A: Civil Engineering
http://scientiairanica.sharif.edu

Soil-structure interaction response considering drift analysis due to three orthogonal components of near-field ground motions

H. Sabermahany and R. Attarnejad*

School of Civil Engineering, College of Engineering, University of Tehran, Tehran, Iran.

Received 26 May 2021; received in revised form 23 December 2021; accepted 25 April 2022

KEYWORDS
Soil-structure interaction;
Seismic performance;
Foundation rocking;
Inter-story drift;
Nonlinear analysis.

Abstract. Soil-structure interaction analysis is one of the most challenging problems in the field of structural engineering. In this paper, two aspects less discussed in the literature, namely: (i) the effect of considering all three components of near-field earthquake excitations instead of just one horizontal component and (ii) elimination of the part of inter-story drifts caused by the foundation rocking, were investigated. Theoretical aspects of both phenomena were considered, and useful considerations were proposed. To provide a more comprehensive description of the suggested modifications, the seismic behavior of a 15-story steel moment-resisting frame building subjected to four near-field earthquake excitations was studied. To this end, 3D nonlinear time-history analysis was conducted using ABAQUS finite element software. The structure is supported by a shallow raft foundation on soft-clayey soil. The results indicate that the two mentioned points are of prime importance and should be considered in the soil-structure interaction analysis due to near-field excitations to evaluate the seismic structural responses more accurately.

1. Introduction

Soil-Structure Interaction (SSI) is referred to the mutual effects of soil and structure behavior on each other. Traditional structural design methods ignore the SSI effects and analyze the structure considering the fixed-base condition. However, studies in the field of SSI have proved that neglecting SSI is not reasonable, except for the case of stiff soil [1–5]. The seismic response of a building can be obtained from 3D nonlinear time-history analysis of the Soil-Foundation-Structure System (SFSS). The substructure method and the direct method are two numerical modeling approaches used to analyze the SFSS. In the substructure method, the SFSS is divided into substructures (usually superstructure and soil-foundation), and suitable restraints (springs and dashpots) are considered at their interface. Finally, the seismic response of the SFSS is calculated based on the principle of superposition. The nonlinear mechanisms involved in SSI problems are not considered completely in the substructure method because the superposition used in this method is based on the assumption of linear behavior [6]. The substructure method has been used in many studies to solve SSI problems [7–14]. Also, the direct method is a powerful method that can consider different nonlinearities involved in SSI problems [15]. Unlike the substructure method, in the direct approach, the whole SFSS is modeled as a unified system. Many researchers have used the direct method to investigate the seismic response

*. *Corresponding author.*
E-mail addresses: hadi.sabermahany@ut.ac.ir (H. Sabermahany); attarnjd@ut.ac.ir (R. Attarnejad)

doi: 10.24200/sci.2022.58423.5716

of structures considering SSI [16–23]. Development of the numerical modeling approaches in the field of SSI has been considered in research over the last few years. González Acosta et al. [24] proposed an implicit material point method, which does not use a mesh to discretize the material unlike the mesh-based methods like the finite element method, to simulate SSI problems. It was demonstrated that the proposed method could simulate realistic SSI behavior. Phuor et al. [25] considered the skew boundary condition for 3D finite element analysis of SSI. The implementation and validation of the method were presented in detail. Longo et al. [26] presented a methodology for SSI analysis following the substructure method. The SFSS was divided into three subsystems: the far-field soil, the near-field soil, and the superstructure along with its foundation, and appropriate interface elements were utilized. The presented model allows the study of extensive variations of the structure.

Previous studies [18–22], which considered the seismic response of SFSS, generally incorporate only one horizontal component of earthquake excitations into the numerical analysis and report the preliminary calculated inter-story drifts. Thus, two important points seem to have been ignored in previous studies. The first point is the analysis of the SFSS subjected to all three components of earthquake excitations. The vertical component could affect the seismic response of the SFSS subjected to near-field ground motions [27]. Also, both horizontal components should be considered in the analysis in order to evaluate the foundation rocking accurately. During earthquake excitations, foundation rocking occurs due to the inertial moments of the foundation and the inertial forces created within the superstructure. These forces generate compressive and tensile stresses in the foundation and, in turn, cause settlement and possible uplift of the foundation on its sides. When the SFSS is analyzed considering both horizontal components of an earthquake excitation, the distribution of compressive and tensile stresses imposed on the foundation at its sides is changed compared to the case that just one horizontal component is considered in the analysis (Figure 1). Therefore, change in the foundation rocking motion subjected to both horizontal components of an excitation compared to the case involving the application of only one horizontal component of that excitation to the model is expected due to the change in the distribution of stresses imposed on the foundation in two cases.

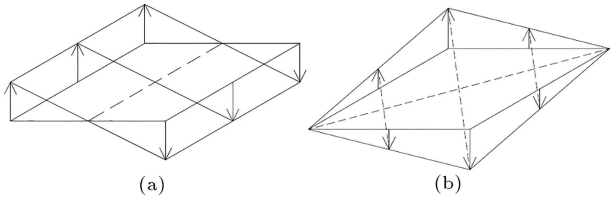

Figure 1. Schematic modeling of distribution of compressive and tensile stresses imposed on the foundation: (a) Due to a uniaxial excitation and (b) due to a biaxial excitation.

The second point is the elimination of the foundation rocking component from the preliminary calculated drifts during the SSI analysis in order to estimate the net inter-story drifts. The rigid body rotation of the building is the result of foundation rocking. Although lateral displacements due to the rigid body rotation should be considered in P-Delta effects during analysis, it should be noted that the rigid body rotation does not directly generate any forces as well as damages in structural and nonstructural members. Thus, considering the second point is reasonable.

Considering the effects of two mentioned points on the seismic response of a 15-story steel moment-resisting frame structure supported by a shallow square raft foundation on soft soil is the aim of this study. To achieve this goal, 3D nonlinear time-history analysis of the SFSS under the influence of four earthquake excitations considering the effects of the two aforementioned points was carried out using ABAQUS software. The direct numerical approach was used in the numerical analysis. Also, the geometric and material nonlinearities were taken into account for the superstructure, foundation, and soil elements.

2. Properties of soil-structure system

2.1. Properties of structure and foundation

A 15-story steel moment-resisting symmetrical building frame was considered in this study (Figure 2). The height of each story is equal to 3 m. The building has a 15 × 15 m floor plan comprised of three 5 m spans in both directions (Figure 2). Also, the building is supported by a shallow square raft foundation of 16.5 × 16.5 m. The foundation slab is located on the ground surface similar to previous studies [20,21]. The material properties of steel members are presented in Table 1. In addition to the self-weight of the floor slabs, the dead load of 1.6 kPa combined with the live load of 2 kPa was uniformly applied over the floors. The structure was designed based on the Iranian seismic code [28]. Also, the shallow raft foundation was designed to support

Table 1. Properties of steel members.

Properties	Value
Density (kg/m^3)	7850
Young's modulus (GPa)	200
Poisson's ratio	0.3
Yield stress, F_y (MPa)	240
Tensile strength, F_u (MPa)	370

Table 2. Designed sections (values are in cm).

Story number	*I*-beam section for beams		Square box section for columns	
	Web	Flange	Width	Thickness
1–4	45 × 0.8	30 × 2	50	3
5–8	40 × 0.8	25 × 2	45	3
9–12	35 × 0.8	25 × 2	40	3
13–15	30 × 0.8	20 × 2	35	3

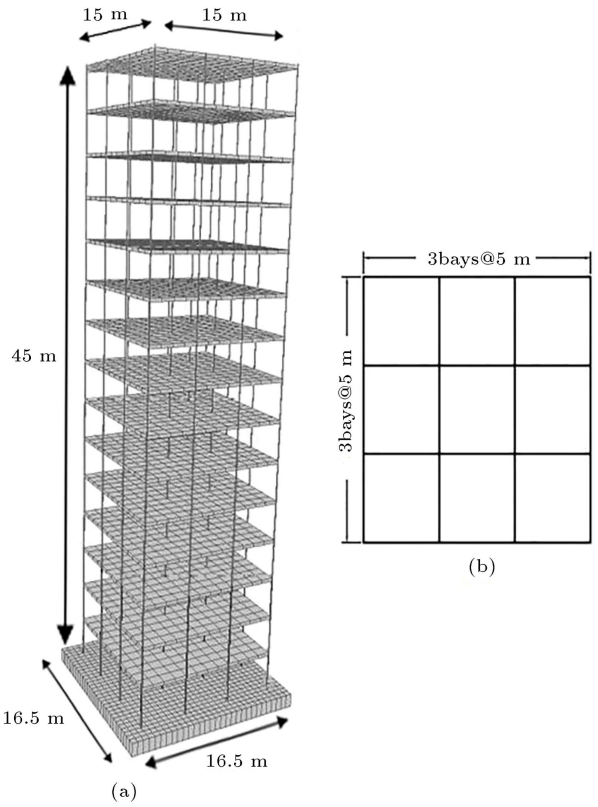

Figure 2. 15-story structure adopted in the numerical model: (a) 3D view and (b) plan of each story.

Table 3. Properties of the concrete floor slabs and foundation.

Properties	Value
Floor slabs thickness (cm)	25
Foundation thickness (m)	1
Density (kg/m^3)	2500
Young's modulus (GPa)	23.5
Poisson's ratio	0.2
Compressive strength (MPa)	25

the structure followed by routine engineering design procedures. Designed sections for the structure are presented in Table 2. Moreover, the characteristics of the concrete floor slabs and foundation are given in Table 3.

Table 4. Soil parameters.

Properties	Value
Density (kg/m^3)	1470
Poisson's ratio	0.4
Maximum shear modulus, $G_{\max}$ (kPa)	33100
Shear wave velocity (m/s)	150
Undrained shear strength, C_u (kPa)	50

2.2. Properties of soil

The superstructure sits on soft-clayey soil, and the properties of this subsoil, extracted from an actual geotechnical project [29], are presented in Table 4.

3. Numerical modeling

The numerical model of the studied SFSS was created using ABAQUS finite element software, and 3D nonlinear time-history analysis of the system was conducted. To that end, the geometric nonlinearity, along with P-Delta effects, was taken into account in the analysis. To consider P-Delta effects in ABAQUS finite element software, gravity loads should be presented during analysis. The analysis was performed in two steps to consider gravity loads during analysis. To this end, the system was analyzed due to the gravity loads in the first step, and then in the second step, the dynamic analysis of the system subjected to the earthquake excitations was conducted. Similar to the structure designing mentioned earlier, the gravity loads during the analysis were equal to the combined sum of the dead loads and 20% of the live loads.

3.1. Structural and foundation models

The 2-node linear beam (B31) elements were utilized to simulate the beam and column members. In addition, the 4-node, reduced integration, quadrilateral shell (S4R) elements and the 8-node, three-dimensional, hourglass control, reduced integration, linear brick (C3D8R) elements were utilized to simulate the floor slabs and foundation, respectively. The inelastic behavior of structural steel elements was modeled using the bilinear kinematic strain hardening of 1%, as recommended by EN 1993-1-5 [30] (Figure 3(a)). The inelastic behavior of structural concrete elements was

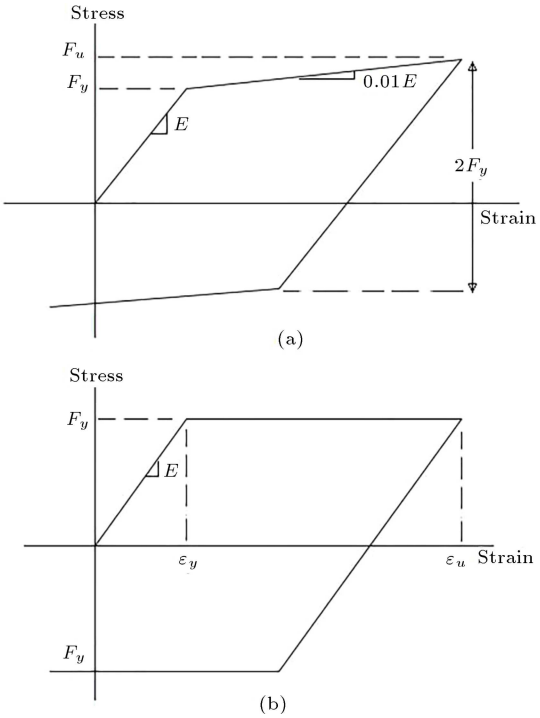

Figure 3. Behavior of structural elements adopted in the numerical model: (a) Steel elements and (b) concrete elements.

modeled using elasto-plastic material behavior similar to previous studies [21,22,31] (Figure 3(b)). According to Shing and Tanabe [31] and as applied in the modeling of previous studies [21,22], the compressive strength of concrete was assumed as the yield stress of concrete material. Yielding and uplift characteristics of the concrete foundation were considered by modeling the inelastic behavior of concrete elements and using appropriate characteristics for the contact at the interface between the soil and foundation surfaces.

Moreover, the damping ratio (ξ) was set at 5% and was taken into account in the definition of structural materials by introducing the Rayleigh damping coefficients. These coefficients are α known as mass proportional coefficient and β known as stiffness proportional coefficient; they are obtained as follows [32]:

$$\alpha = \xi \frac{4\pi f_i f_j}{(f_i + f_j)}; \quad \beta = \xi \frac{1}{\pi (f_i + f_j)},$$
$$\xi = \frac{\alpha}{4\pi f_i} + \beta \pi f_i, \tag{1}$$

where f_i is the frequency of mode i and f_j is the frequency of mode j. Using Eq. (1) and based on the frequencies of the first two modes obtained at 0.56 Hz and 1.6 Hz for the studied structure from the frequency analysis of the fixed-base structure, the Rayleigh damping coefficients, α and β, were obtained equal to 0.261 and 0.0073, respectively.

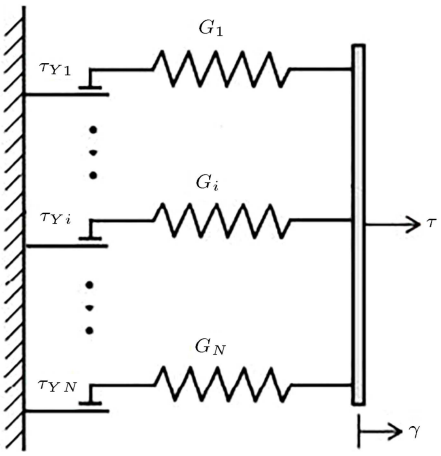

Figure 4. Schematic representation of multiple parallel elasto-plastic elements used in the overlay model.

3.2. Soil model

The overlay model was utilized in this study to model the hysteresis behavior of soil elements. N parallel elasto-plastic elements known as overlay elements are used in this model to achieve the nonlinear behavior of a soil element (Figure 4). Every element of parallelelements (denoted i) behaves elastically at strains less than γ_i with shear modulus G_i and behaves perfectly plastic with the yield stress τ_{Yi} at strains exceeding γ_i.

The stress-strain behavior is defined below using overlay elements:

$$\tau(\gamma) = \sum_{i=1}^{n} G_i \gamma + \sum_{i=n+1}^{N} \tau_{Yi}, \tag{2}$$

where τ is shear stress, γ is shear strain, and n is the number of parallel elements that behave elastically based on the given shear strain. The yield stress and the shear modulus of overlay elements were specified by Kaklamanos [33] and presented in appendix. Eq. (2) indicates that the backbone curve, which specifies the stress-strain behavior, is obtained with a multi-linear curve (Figure 5). In fact, the obtained backbone

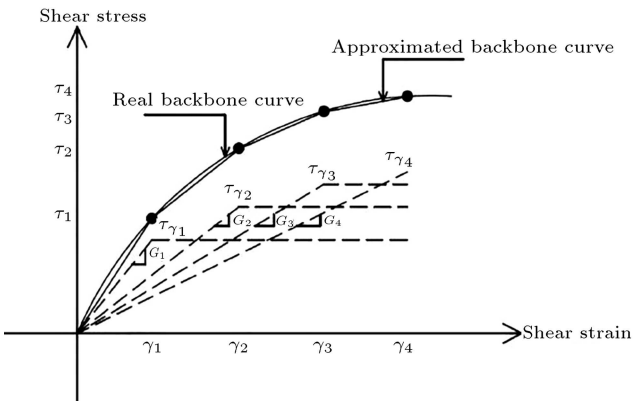

Figure 5. Real backbone curve and the approximated backbone curve of the overlay model for $N = 4$.

curve of the overlay model is composed of N linear segments. Using the overlay model, each backbone curve with any form is obtained with due accuracy. Obviously, a backbone curve is achieved with higher accuracy using more overlay elements, where more computational effort is required.

Using the overlay model, the hysteresis behavior of soil elements is obtained based on the extended Masing behavior, and the hysteretic damping is taken into account in the analysis automatically [34]. Dawson et al. [35] specified that the hysteretic behavior of soil elements in orthogonal directions under the influence of simultaneous cyclic loading could be simulated by the use of the overlay model.

The hysteretic damping ratio and the backbone curve are determined using Eq. (3) and Eq. (4), respectively [33]:

$$\xi(\gamma_a) = \frac{2}{\pi}\left(\frac{2\int_0^{\gamma_a}\tau(\gamma)\,d\gamma}{\gamma_a\tau_a} - 1\right), \tag{3}$$

$$\tau(\gamma) = G_{\max}\left(\frac{G}{G_{\max}}(\gamma)\right)\gamma, \tag{4}$$

where γ_a and τ_a are the shear strain and stress values of point a. In Eq. (4), the modulus-reduction curve ($G/G_{\max}$) indicates the shear modulus variations with the soil cyclic shear strain. In this study, the mathematical expression suggested by Stokoe et al. [36] (Eq. (5)) was utilized for the modulus-reduction curve:

$$\frac{G}{G_{\max}}(\gamma) = \frac{1}{1+\left(\frac{\gamma}{\gamma_r}\right)^{\alpha}}, \tag{5}$$

where γ_r is the reference strain and is equal to the shear strain when $G/G_{\max} = 0.5$. Also, α is the curvature parameter.

Figure 6 shows two calculated modulus-reduction curves along with the modulus-reduction curve obtained for cohesive soils by Sun et al. [37] through the resonant column test. The reference strain was set to 0.234% for both calculated modulus-reduction curves. Moreover, Figure 7 indicates the variations of the damping ratio with shear strains. The calculated curves in Figure 7 were obtained using Eq. (3). Furthermore, the integral of Eq. (3) was calculated using the multi-linear approximated curve of the overlay model. Also, N was chosen equal to 7 in this study. The hysteretic damping is almost zero at small strains because the soil elements behave almost elastically at small strains. Therefore, the damping ratios at small strains are equal to zero in the calculated curves of Figure 7. The user can define viscous damping to maintain damping at small strains. Figure 6 indicates that Eq. (5) is an appropriate expression for the modulus-reduction curve of cohesive soils with γ_r and α equal to 0.234% and 0.7, respectively. Also, Figure 7 specifies that the backbone curve is obtained with due accuracy using the overlay model.

In a finite element software, N parallel elements per each soil element should be defined to apply the overlay model. N parallel elements have the same strain, and the summation of their stresses is the stress of the ensemble. To define N parallel elements in finite element software, N elements with identical nodes should be defined. These N elements have equal strain components because the displacement components, and in turn, the strain components are defined based on the element nodes. Also, the stress components of the ensemble are equal to the sum of the stress components of these N elements. In ABAQUS, the user can define N elements with identical nodes by modifying the input text file. The user should create the model and request the input text file. Then, for each existing soil element in the input file, the user should define $N-1$ new soil elements using the nodes of that element. In fact, the existing soil elements in the input text file are considered as the first overlay element set, and the user should define $N-1$ new overlay element sets. Then, the modified input text file should be exported to ABAQUS

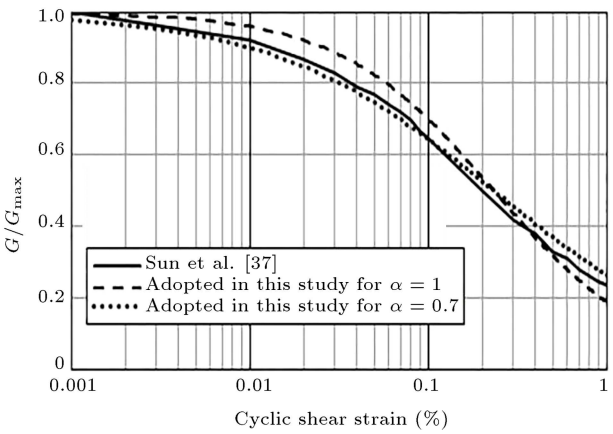

Figure 6. Modulus-reduction curves.

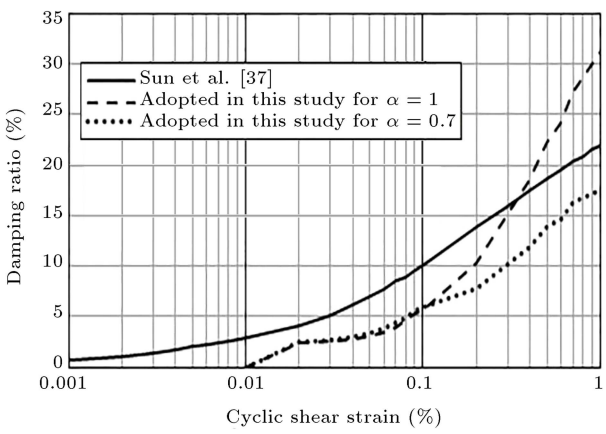

Figure 7. Variations of damping ratio with shear strain.

to achieve a new model. This process was conducted in this study. The soil medium was simulated using C3D8R elements. Moreover, N materials were defined in order to assign them to N overlay element sets. The properties of these N materials are as follows:

$$\rho_1 = \rho_2 = ... = \rho_N = \frac{\rho}{N}, \tag{6}$$

$$\nu = \nu_1 = \nu_2 = ... = \nu_N, \tag{7}$$

$$E_i = 2G_i\left(1 + \nu_i\right), \tag{8}$$

where ρ is the density and ν is the Poisson's ratio of soil. Also, Gi is presented in the appendix. For overlay elements in 3D analysis, it is better to use the Tresca yield criterion because the backbone curve is the relation between shear stress and shear strain. Therefore, the Mohr-Coulomb model, one of the plasticity models in ABAQUS, was used to define the plasticity for each of these N materials. The friction angle and the dilation angle were defined zero for each of these N materials. Hence, the Tresca yield criterion is used [38]. Furthermore, τ_{Yi} presented in the appendix was used in the Mohr-Coulomb model as the cohesion yield stress.

Here, the numerical modeling of a performed test by Hokmabadi [39] was investigated using the overlay model. A laminar soil container filled with soil was tested on a shaking table subjected to shaking events in this test. The depth, length, and width of the container were 1.1 m, 2.1 m, and 1.3 m, respectively. The properties of the soil mix in the test are presented in Table 5.

The overlay model was used to model the nonlinear behavior of soil elements in numerical modeling. N was equal to 7. The modulus-reduction curve of Eq. (5) was used in which the reference strain was set to 0.234% and two values were considered for the curvature parameter. The rigid boundary condition was utilized beneath the soil medium. In addition, the tied boundary condition, obtained by constraining the boundary nodes at the same elevation in two orthogonal horizontal directions, was used. The maximum deflection of soil layers with different heights under the influence of the scaled Kobe earthquake is shown in Figure 8.

Table 5. Soil parameters of the performed test by Hokmabadi [39].

Properties	Value
Density (kg/m^3)	1450
Poisson's ratio	0.44
Maximum shear modulus, $G_{\max}$ (kPa)	1776
Shear wave velocity (m/s)	36
Undrained shear strength, C_u (kPa)	3.1

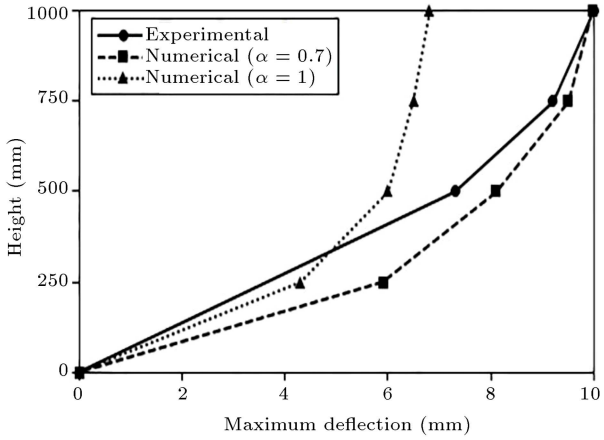

Figure 8. Maximum deflection of soil layers due to the scaled Kobe earthquake.

The scaled record was obtained by dividing the time intervals of the original record by the scale factor, which was 5.48 for the studied shaking table test (Figure 9). Figure 8 indicates that the numerical and experimental results are obtained close to each other when the curvature parameter is equal to 0.7.

3.3. Boundary conditions

The soil lateral boundaries were placed such that the horizontal distance of these boundaries would be equal to six times the dimension of the foundation, which is consistent with the recommendation of previous studies [19,40]. Also, the thickness of the soil profile was chosen to be 30 m. The water table was assumed to be below the level of bedrock. The areas around the lateral boundaries were modeled using infinite elements (Figure 10). Also, an infinite element layer was placed at the soil bottom boundary, where the input excitations were applied (Figure 10). In ABAQUS, infinite elements are provided for use in problems defined with unbounded domains [38]. These elements, which are used in conjunction with finite elements, provide stiffness in static analyses and quiet boundaries in dynamic analyses [38]. It should be noted that only materials with linear behavior can be assigned to infinite elements [38]. In this study, CIN3D8 elements (8-node linear, one-way infinite elements) were used as infinite elements. Also, the length of infinite elements is chosen to be 20 m similar to previous studies [21,22].

3.4. Contact surface

The surface-based contact was used to simulate the interface between the soil and foundation surfaces. The soil top surface was chosen as the master surface, while the foundation bottom surface was chosen as the slave surface. Also, the tangential behavior of the contact surface was modeled using the penalty method. The friction coefficient was chosen equal to 0.3, which is an appropriate value for the friction induced between concrete and clay soil according to the NAVFAC DM-

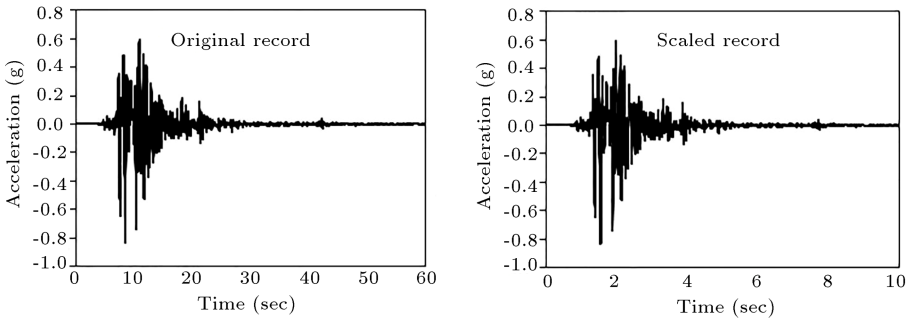

Figure 9. Original and scaled Kobe earthquake records.

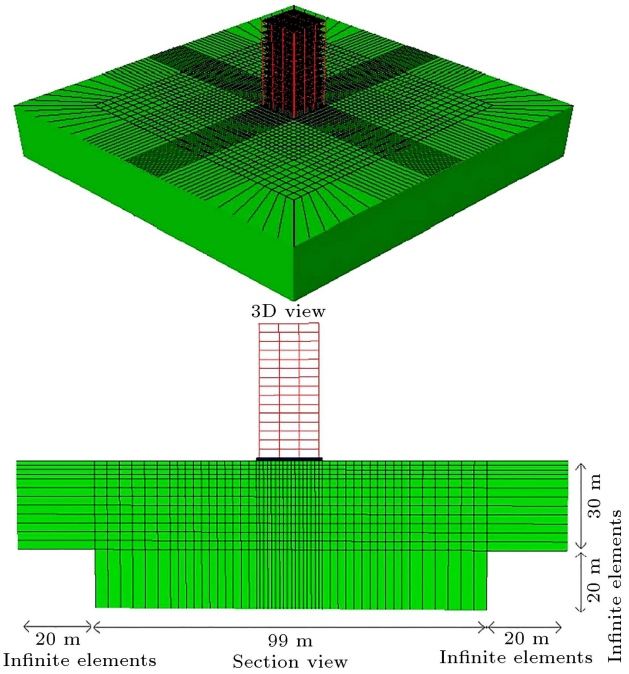

Figure 10. Soil-structure system.

7.2 [41]. In addition, the undrained shear strength of soil (C_u) was defined as the shear stress limit in the penalty method. Moreover, the normal behavior of the contact surface was modeled using the 'hard' contact for the pressure-over closure relationship and, also, using the 'penalty method' as the constraint enforcement method. Therefore, the contact pressure between the master surface and the slave surface is generated just when contact exists between the nodes of two surfaces and the magnitude of the contact force is linearly proportional to the amount of the penetration distance [38]. The 'allow separation after contact' option was used to capture any possible uplift of the foundation.

3.5. Input ground motion records

Four near-field earthquake excitations were considered as input ground motion records. Table 6 lists the characteristics of these earthquake excitations, which were taken from the PEER NGA database [42]. The near-field earthquake excitations, which generally have a strong vertical component, were selected because the effects of the vertical component of excitations, as well as the horizontal components, on the seismic response of the system are to be investigated. For each earthquake excitation, two analysis cases were considered. In analysis case 1, just the acceleration time history of the X-component of each earthquake excitation was applied to the model. On the other hand, acceleration time histories of both horizontal components along with the acceleration time history of the vertical component of each earthquake excitation were imposed onto the numerical model in analysis case 2.

Between the two horizontal components of each earthquake excitation, the one that causes a larger roof displacement was selected as the X-component.

The soil medium consisted of 40,508 nodes and 31,212 elements based on the generated mesh specified in Figure 10. By modifying the initial input text file in a way described in the overlay model, 187,272 ($(N-1)\times 31,212 = 6\times 31,212 = 187{,}272$) new soil elements were defined using the nodes of the existing soil elements in the initial input text file. The computational facilities at the Civil Engineering Department at the University

Table 6. Utilized earthquake excitations.

Earthquake	Year	Station	PGA of X-component (g)	Significant duration (sec)	Predominant frequency (Hz)
Irpinia	1980	Sturno (STN)	0.32	20.00	5.00
Loma Prieta	1989	LGPC	0.57	17.50	1.42
Northridge	1994	Jensen Filter Plant	0.41	15.50	0.98
Tabas	1978	Tabas	0.86	22.50	5.00

of Tehran were used to carry out 3D nonlinear time-history analyses. The results of these analyses are presented and discussed in the following section.

4. Results and discussions

Figure 11 shows the relative lateral displacement along the x-axis for the center of mass of all stories for two cases of analysis. The values presented in Figure 11 are the lateral displacement of stories relative to the foundation movement when the maximum relative displacement of the roof story occurred. It should be noted that the presented relative displacements include the contribution due to foundation rocking. Also, Table 7 shows the percentage difference in relative lateral displacements obtained from cases 1 and 2 of analysis for the 5th and 10th stories, and Table 8 presents the maximum roof relative displacement for two cases of analysis. Figure 11 indicates that the relative lateral displacement of stories increases by applying all three components of earthquake excitations (analysis case 2) instead of applying only the X-component of earthquake excitations (analysis case 1). Also, Figure 11 specifies that the absolute difference between the relative lateral displacements obtained from cases 1 and 2 of analysis generally increases by increasing the number of stories. On the other hand, Table 7 shows that the percentage difference in relative lateral displacements obtained from cases 1 and 2 of analysis is almost the same for the 5th and 10th stories. Moreover, Table 8 shows that the maximum roof relative displacement obtained from case 2 of analysis is, on average, 25% larger than the value obtained from case 1 of analysis. It should be noted that estimating the lateral displacements, especially the roof lateral displacement, more accurately leads to better consideration of the possible structural seismic pounding.

The relative lateral displacement of the structure in the SSI analysis is composed of structural distortion and rocking components (Figure 12). Structural distortion is directly dependent on the shear forces generated in the structure. The generated shear forces in the structure and the foundation rocking obtained from

Table 7. The percentage difference in relative lateral displacements obtained from cases 1 and 2 of analysis for the 5th and 10th stories.

Earthquake	Percentage difference (%)	
	5th story	10th story
Irpinia	35.00	34.76
Loma Prieta	12.06	11.61
Northridge	21.34	22.75
Tabas	35.79	35.58

Table 8. Maximum roof relative displacements obtained from two cases of analysis.

Earthquake	Roof displacement (cm)	
	Analysis case 1	Analysis case 2
Irpinia	34.68	49.32
Loma Prieta	66.06	69.13
Northridge	52.36	64.45
Tabas	48.51	69.04
Average	**50.40**	**62.99**

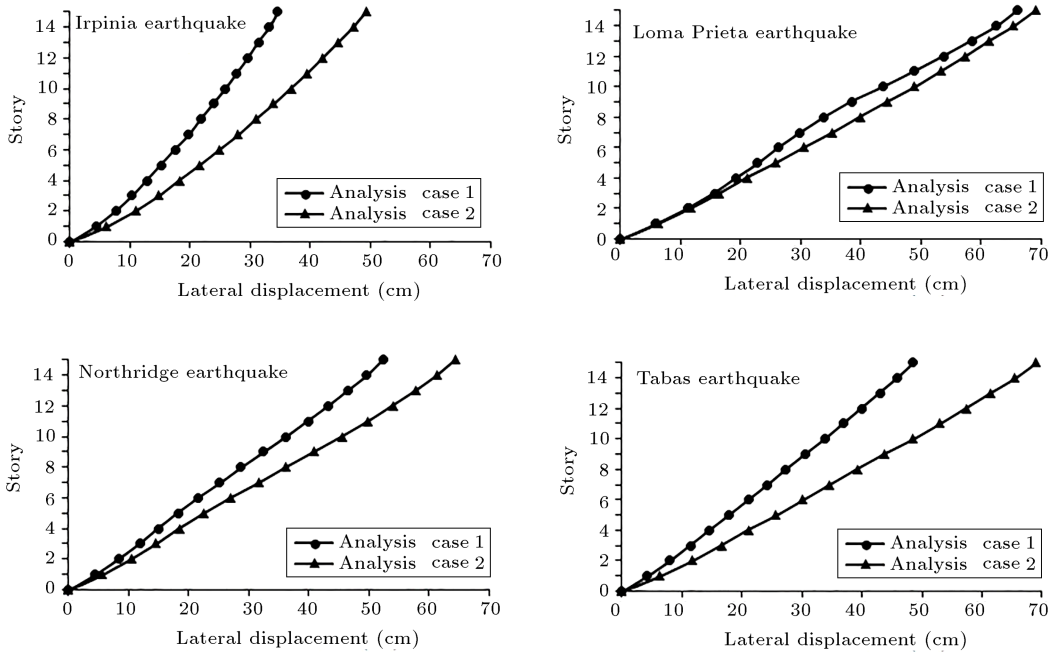

Figure 11. Relative lateral displacement of all stories for two different cases of analysis.

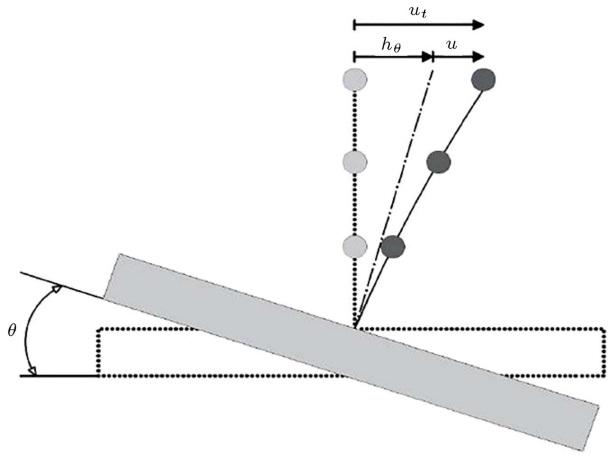

Figure 12. Schematic modeling of relative lateral displacement of superstructure.

case 1 of analysis are compared to those obtained from case 2 of analysis to consider the reason of the difference seen between the relative lateral displacements obtained from these cases of analysis.

Figure 13 shows the maximum shear force in all stories of the superstructure for two different analysis cases. The shear force in each story at every increment of analysis is equal to the sum of the shear forces generated in all columns of that story.

Referring to Figure 13, a specific trend has not been found between the shear forces obtained from cases 1 and 2 of analysis, and the maximum generated shear forces of stories obtained from these two cases of analysis are generally close to each other.

The time history response of the foundation rocking angle around the y-axis (the y-axis is perpendicular to the x-axis, and relative displacements along the x-axis are considered) is presented in Figure 14 for two cases of analysis. Also, the results of the performed analyses for the maximum foundation rocking angle are presented in Table 9. To this end, the foundation rocking angle was determined by subtracting the vertical displacements of the foundation edges and, then, dividing the obtained value by the width of the foundation at every increment of analysis. As illustrated earlier, the foundation rocking occurs due to the compressive and tensile stresses imposed on the foundation at its sides during earthquake excitations. These stresses are originated from the generated inertial forces within the structure. The distribution of these stresses on the foundation at its sides can be actually influenced by the existence of both horizontal components of earthquake excitations at the same time, as well as the existence of the vertical component, in case 2 of analysis. Therefore, the foundation rocking angles obtained from case 2 of analysis are different from those obtained from case 1 of analysis (Figure 14 and Table 9). The influence of excitation components on the

Table 9. Maximum foundation rocking angles obtained from two different cases of analysis.

Earthquake	Foundation rocking angle (degree)	
	Analysis case 1	**Analysis case 2**
Irpinia	0.24	0.30
Loma Prieta	0.55	0.57
Northridge	0.40	0.49
Tabas	0.42	0.58
Average	**0.40**	**0.49**

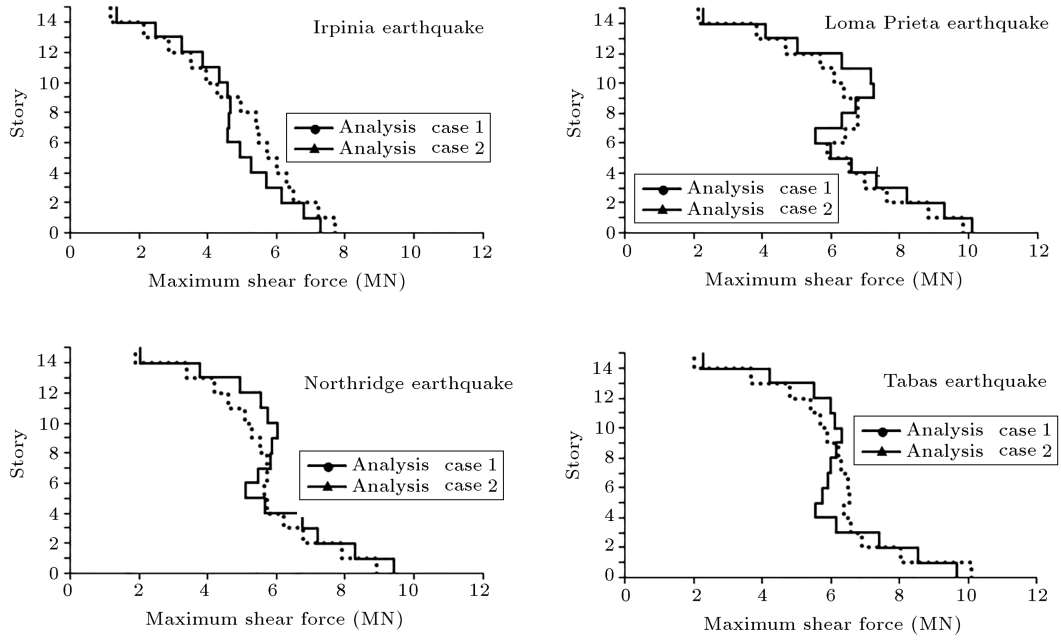

Figure 13. Maximum shear force of all stories for two different cases of analysis.

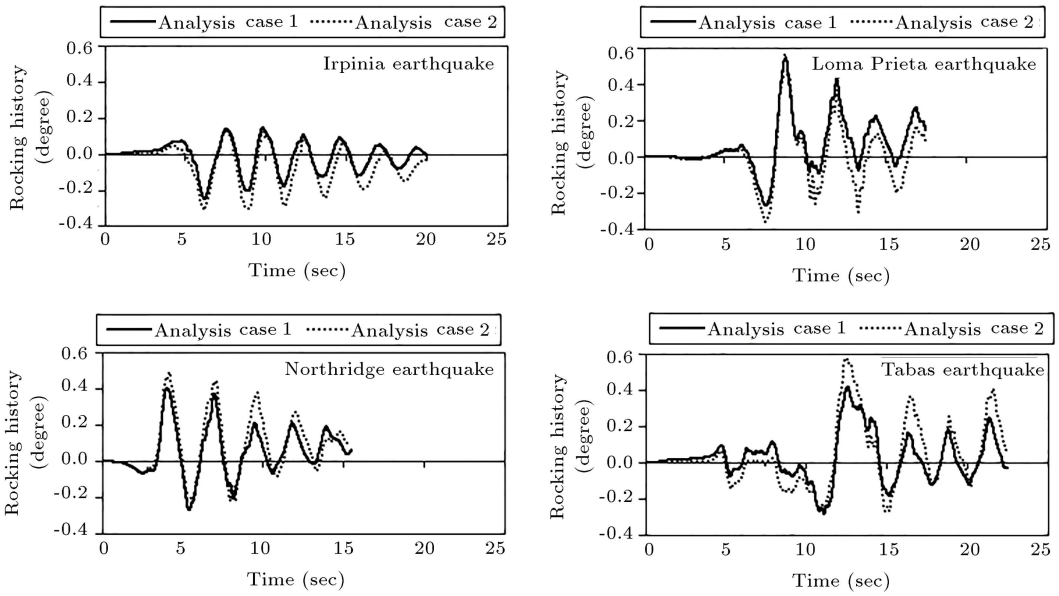

Figure 14. Time history response of foundation rocking angle for two different cases of analysis.

distribution of stresses on the foundation is basically dependent on the excitation components. Therefore, the difference in the maximum foundation rocking angle between cases 1 and 2 of analysis varies between the earthquake excitations considered in this study (see Table 9).

Table 9 indicates that the maximum foundation rocking angle determined from case 2 of analysis is, on average, 22.5% larger than the maximum rocking angle determined from case 1 of analysis. Therefore, the difference between the relative lateral displacements obtained from cases 1 and 2 of analysis is related to the difference between the foundation rocking angles obtained from these two cases of analysis. The contribution of the rocking component is more in the lateral displacement of a story when that story is located at a higher level. So, the absolute difference between the lateral displacements obtained from cases 1 and 2 of analysis would be greater for upper stories, as specified in Figure 11.

The inter-story drifts of the building can be defined using the following equation presented in seismic codes:

$$Drift = \frac{(d_i - d_{i-1})}{H_i}, \tag{9}$$

where d_i and d_{i-1} are the relative lateral displacements at i and $i-1$ levels, respectively. Moreover, H_i is the story height. As illustrated earlier, the relative lateral displacement of the structure is composed of structural distortion and rocking components when the SSI is considered in the analysis. Thus, we have:

$$d_i = u_i + h_i\theta, \tag{10}$$

where u_i is the structural distortion at level i, h_i is the height of level i from the foundation level, and θ is the foundation rocking angle. Therefore, the inter-story drifts calculated based on Eq. (9) contain the rigid body rotation (rocking) component. The rigid body rotation of the building affects the P-Delta analysis, but does not directly induce any damages in the structural and nonstructural members. Thus, the rigid body rotation component should be eliminated from Eq. (9) to define the net inter-story drifts. Using Eqs. (9) and (10), the following equation is obtained:

$$\begin{aligned} Drift &= \frac{(u_i + h_i\theta - u_{i-1} - h_{i-1}\theta)}{H_i} \\ &= \frac{(u_i + (h_{i-1} + H_i)\,\theta - u_{i-1} - h_{i-1}\theta)}{H_i} \\ &= \frac{(u_i - u_{i-1})}{H_i} + \theta. \end{aligned} \tag{11}$$

In this study, the preliminary calculated inter-story drift determined based on Eq. (9) is specified as the initial drift, and the inter-story drift obtained after elimination of the rocking component is specified as the net drift. Therefore, the value of the net drift is equal to the value of the initial drift minus the value of the rocking angle (see Eq. (11)).

Figures 15 and 16 show the maximum inter-story drifts for cases 1 and 2 of analysis, respectively. Both of the initial and net drifts are presented for the soil-foundation-structure interaction analysis. Table 10 indicates the percentage difference between the maximum initial and net inter-story drifts obtained from cases 1 and 2 of analysis for the 4th, 8th, and 12th stories. As specified in Figures 15 and 16 along with Table 10, the difference between the initial and net inter-

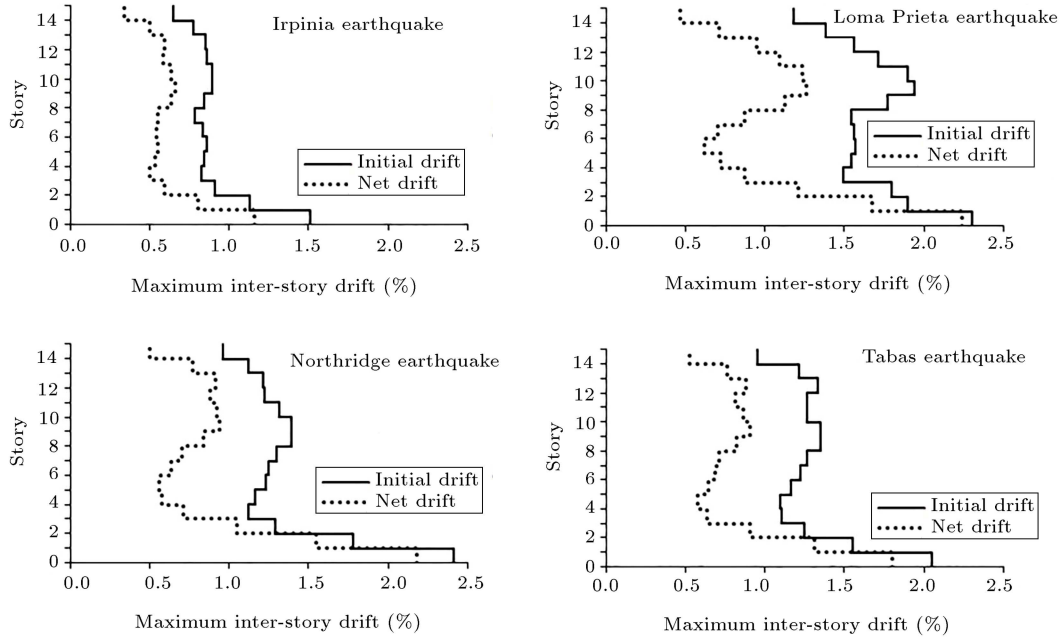

Figure 15. Maximum initial and net inter-story drifts of all stories for case 1 of analysis.

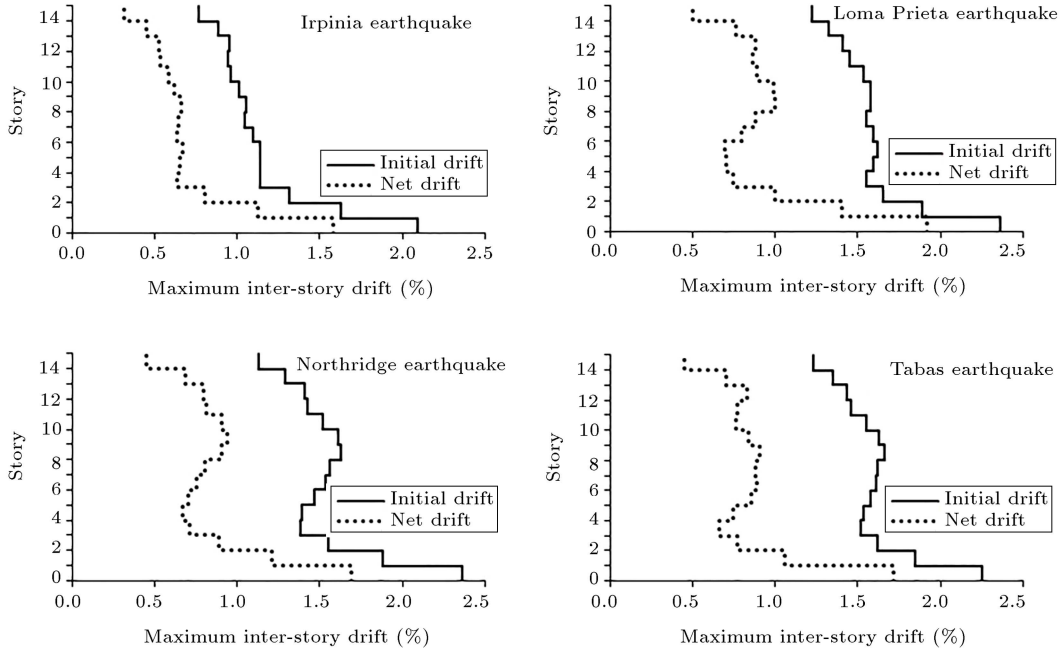

Figure 16. Maximum initial and net inter-story drifts of all stories for case 2 of analysis.

Table 10. The percentage difference between the maximum initial and net inter-story drifts obtained from cases 1 and 2 of analysis for the 4th, 8th, and 12th stories.

Earthquake	Percentage difference (%)					
	4th story		8th story		12th story	
Irpinia	48.48	57.63	34.59	47.62	38.89	55.78
Loma Prieta	52.54	70.74	55.60	56.14	44.29	51.08
Northridge	44.81	64.11	60.00	64.41	32.38	54.71
Tabas	54.34	78.90	55.84	59.20	43.48	61.88

story drifts is considerable. Hence, it is important to eliminate the rigid body rotation component from the initial inter-story drift in the soil-foundation-structure interaction analysis, which has not been considered in most of the previous studies. Based on Table 10 and also by comparing Figure 15 with Figure 16, it is seen that differences between the initial and net drifts for case 2 of analysis are greater than those for case 1. The reason for this observation is that the foundation rocking angles obtained from case 2 of analysis are greater than those obtained from case 1.

As seen in Figures 15 and 16, the maximum inter-story drift, derived from the SSI analysis, appears in the first story. Previous studies have also mentioned that the maximum inter-story drift appears on the first floor of the moment-resisting frame buildings constructed on soft soil when the SSI was considered in the analysis [10,43–45]. Also, researchers have demonstrated that base flexibility resulted in the large displacement of the first story [46,47]. Therefore, the lateral displacements of the first story in moment-resisting frame structures could increase significantly in the SSI analysis due to base flexibility, which originates from soil-foundation flexibility in the SSI analysis. Therefore, base flexibility should be decreased in order to reduce the maximum net inter-story drift and improve the seismic performance of the structure. To that end, base flexibility can be decreased by modifying the soil or the characteristics of the foundation to increase the stiffness of the soil-foundation system.

5. Conclusions

3D nonlinear time-history analysis of a soil-foundation-structure system with a 15-story steel moment-resisting frame building supported by a shallow raft footing on soft-clayey soil was implemented due to four near-field earthquake excitations. Two cases of analysis were performed. In case 1, only one horizontal component of earthquake excitations was considered in the analysis. However, in case 2, all three components of earthquake excitations were considered in the analysis. The following conclusions were obtained from the numerical investigations performed in this study:

- The maximum foundation rocking angle due to all three components of ground motions (triaxial excitations) was larger than the maximum rocking angle due to only one horizontal component of ground motions;
- The maximum shear forces of stories subjected to all three components of ground motions were close to those obtained due to just one horizontal component of ground motions;
- Considering all three components instead of just one horizontal component of ground motions in the analysis leads to the increase of the relative lateral displacements of stories. While the percentage difference between the relative lateral displacements obtained from two cases of analysis is almost the same for different stories, the absolute difference between the mentioned lateral displacements increases by increasing the number of stories. Therefore, all three components of ground motions should apply to the soil-foundation-structure system during analysis in order to determine the lateral displacements, especially the roof lateral displacement, in a more accurate manner;
- Net inter-story drifts during the Soil-Structure Interaction (SSI) analysis were determined by eliminating the part of inter-story drifts caused by the foundation rocking from the preliminary calculated drifts (initial drifts). The difference between the initial and net inter-story drifts is considerable and the maximum net inter-story drift should be considered to determine the seismic performance of structures logically. Also, differences between the initial and net drifts for case 2 of analysis are greater than those for case 1;
- It is verified that the maximum drift of the studied structure obtained from the SSI analysis is located in the first story, and this point should be given careful consideration to ensure a safe seismic design.

References

1. Mylonakis, G. and Gazetas, G. "Seismic soil-structure interaction: Beneficial or detrimental?", *Journal of Earthquake Engineering*, **4**(3), pp. 277–301 (2000).
2. Galal, K. and Naimi, M. "Effect of soil conditions on the response of reinforces concrete tall structures to near-fault earthquakes", *The Structural Design of Tall and Special Buildings*, **17**(3), pp. 541–562 (2008).
3. Tabatabaiefar, S.H.R., Fatahi, B., and Samali, B. "Seismic behavior of building frames considering dynamic soil-structure interaction", *International Journal of Geomechanics*, **13**(4), pp. 409–420 (2013).
4. Anand, V. and Satish Kumar, S.R. "Seismic soil-structure interaction: A state-of-the-art review", *Structures*, **16**, pp. 317–326 (2018).
5. Jia, F., Jianwen, L., and Zhenning, B. "Model errors caused by rigid foundation assumption in soil structure interaction: a comparison of responses of a soil structure flexible foundation system and a rigid foundation system", *Bulletin of Earthquake Engineering*, **19**, pp. 77–99 (2021).
6. Jabini Asli, S., Saffari, H., Zahedi, M.J., et al. "Comparing the performance of substructure and direct

methods to estimate the effect of SSI on seismic response of mid-rise structures", *International Journal of Geotechnical Engineering*, **15**(1), pp. 81–94 (2021).

7. Rajeev, P. and Tesfamariam, S. "Seismic fragilities of non-ductile reinforced concrete frames with consideration of soil structure interaction", *Soil Dynamics and Earthquake Engineering*, **40**, pp. 78–86 (2012).

8. Minasidis, G., Hatzigeorgiou, G.D., and Beskos, D.E. "SSI in steel frames subjected to near-fault earthquakes", *Soil Dynamics and Earthquake Engineering*, **66**, pp. 56–68 (2014).

9. Abdel Raheem, S.E., Ahmed, M.M., and Alazrak, T.M.A. "Evaluation of soil-foundation-structure interaction effects on seismic response demands of multistory MRF buildings on raft foundations", *International Journal of Advanced Structural Engineering*, **7**(1), pp. 11–30 (2015).

10. Behnamfar, F. and Banizadeh, M. "Effects of soil-structure interaction on distribution of seismic vulnerability in RC structures", *Soil Dynamics and Earthquake Engineering*, **80**, pp. 73–86 (2016).

11. Tahghighi, H. and Rabiee, M. "Influence of foundation flexibility on the seismic response of low-to-mid-rise moment-resisting frame buildings", *Scientia Iranica*, **24**(3), pp. 979–992 (2017).

12. Shakib, H. and Homaei, F. "Probabilistic seismic performance assessment of the soil-structure interaction effect on seismic response of mid-rise setback steel buildings", *Bulletin of Earthquake Engineering*, **15**, pp. 2827–2851 (2017).

13. Deng, H.Y., Jin, X.Y., and Gu, M. "A simplified method for evaluating the dynamic properties of structures considering soil-pile-structure interaction", *International Journal of Structural Stability and Dynamics*, **18**(6), 1871005 (2018). https://Doi.org/10.1142/S0219455418710050

14. Asadi-Ghoozhdi, H. and Attarnejad, R. "The effect of nonlinear soil-structure interaction on the ductility and strength demands of vertically irregular structures", *International Journal of Civil Engineering*, **18**, pp. 1209–1228 (2020).

15. Far, H. "Advanced computation methods for soil-structure interaction analysis of structures resting on soft soils", *International Journal of Geotechnical Engineering*, **13**(4), pp. 352–359 (2019).

16. Borja, R.I., Chao, H.Y., Montáns, F.J., et al. "SSI effects on ground motion at Lotung LSST site", *Journal of Geotechnical and Geoenvironmental Engineering*, **125**(9), pp. 760–770 (1999).

17. Mirhashemian, P., Khaji, N., and Shakib, H. "Soil-structure interaction (SSI) analysis using a hybrid spectral element/finite element (SE/FE) approach", *Journal of Seismology and Earthquake Engineering* (JSEE), **11**(2), pp. 83–95 (2009).

18. Tabatabaiefar, S.H.R., Fatahi, B., and Samali, B. "Lateral seismic response of building frames considering dynamic soil-structure interaction effects", *Structural Engineering and Mechanics*, **45**(3), pp. 311–321 (2013).

19. Tabatabaiefar, S.H.R., Fatahi, B., and Samali, B. "An empirical relationship to determine lateral seismic response of mid-rise building frames under influence of soil-structure interaction", *The Structural Design of Tall and Special Buildings*, **23**(7), pp. 526–548 (2014).

20. Hokmabadi, A.S. and Fatahi, B. "Influence of foundation type on seismic performance of buildings considering soil-structure interaction", *International Journal of Structural Stability and Dynamics*, **16**(8), 1550043 (2016). https://doi.org/10.1142/S0219455415500431

21. Nguyen, Q.V., Fatahi, B., and Hokmabadi, A.S. "The effects of foundation size on the seismic performance of buildings considering the soil-foundation-structure interaction", *Structural Engineering and Mechanics*, **58**(6), pp. 1045–1075 (2016).

22. Nguyen, Q.V., Fatahi, B., and Hokmabadi, A.S. "Influence of size and load-bearing mechanism of piles on seismic performance of buildings considering soil-pile-structure interaction", *International Journal of Geomechanics*, **17**(7), 04017007 (2017). https://doi.org/10.1061/(ASCE)GM.1943-5622.0000869

23. Shahbazi, S., Khatibinia, M., Mansouri, I., et al. "Seismic evaluation of special steel moment frames subjected to near-field earthquakes with forward directivity by considering soil-structure interaction effects", *Scientia Iranica*, **27**(5), pp. 2264–2282 (2020).

24. González Acosta, J.L., Vardon, P.J., and Hicks, M.A. "Study of landslides and soil-structure interaction problems using the implicit material point method", *Engineering Geology*, **285**, p. 106043 (2021).

25. Phuor, T., Harahap, I.S.H., Ng, C.Y., et al. "Development of the skew boundary condition for soil-structure interaction in three-dimensional finite element analysis", *Computers and Geotechnics*, **137**, p. 104264 (2021).

26. Longo, M., Sousamli, M., Korswagen, P.A., et al. "Substructure-based 'three-tiered' finite element approach to soil-masonry-wall interaction for light seismic motion", *Engineering Structures*, **245**, p. 112847 (2021).

27. Abdollahiparsa, H., Homami, P., and Khoshnoudian, F. "Effect of vertical component of an earthquake on steel frames considering soil-structure interaction", *KSCE Journal of Civil Engineering*, **20**(7), pp. 2790–2801 (2016).

28. Standard No. 2800 "Iranian code of practice for seismic resistance design of buildings", 4th Ed, Ministry

of Road, Housing and Urban Development, Tehran (2014).

29. Rahvar "Geotechnical investigation and foundation design report of Mahshahr train station", P.O. Rahvar Pty Ltd, Iran Railway Authority, Mahshar (2006).
30. EN 1993-1-5: Eurocode 3 "Design of steel structures - Part 1-5: General rules-Plated structural elements", Authority: The European Union Per Regulation 305/2011, Directive 98/34/EC, Directive 2004/18/EC (2006).
31. Shing, B.P. and Tanabe, T. "Modeling of inelastic behavior of RC structures under seismic loads", Reston, VA: American Society of Civil Engineers (ASCE) (2001).
32. Chopra, A.K., *Dynamics of Structures*, Prentice Hall, New Jersey (2007).
33. Kaklamanos, J. "Quantifying uncertainty in earthquake site response models using the KiK-net database", Dissertation, Tufts University (2012).
34. Kaklamanos, J., Dorfmann, L., and Baise, L.G. "A simple approach to site-response modeling: the overlay concept", *Seismological Research Letters*, **86**(2A), pp. 413–423 (2015).
35. Dawson, E., Roth, W., and Su, B. "3-D masing behavior of a parallel Iwan model", *Second International Conference on Geotechnical and Earthquake Engineering*, Chengdu, China (2013).
36. Stokoe, K.H., Darendeli, M.B., Andrus, R.D., et al. "Dynamic soil properties: Laboratory, field and correlation studies", *Second International Conference on Earthquake Geotechnical Engineering*, Lisbon, Portugal (1999).
37. Sun, J., Golesorkhi, R., and Seed, H.B. "Dynamic moduli and damping ratio for cohesive soils", Earthquake Engineering Research Center, University of California Berkeley (1988).
38. ABAQUS, Abaqus Analysis User's Manual, Minneapolis, Minnesota, Dassault Systémes Simulia Corp., USA (2012).
39. Hokmabadi, A.S. "Effect of dynamic soil-pile-structure interaction on seismic response of mid-rise moment resisting frames", Dissertation, University of Technology Sydney (UTS) (2014).
40. Rayhani, M.H.T. and El Naggar, M.H. "Numerical modeling of seismic response of rigid foundation on soft soil", *International Journal of Geomechanics*, **8**(6), pp. 336–346 (2008).
41. Naval Facilities Engineering Command, Design Manual 7.02, "Foundation & earth structures", Alexandria, Virginia (1986).
42. PEER, Pacific Earthquake Engineering Research center strong motion database (2014). http://peer.berkeley.edu
43. Zhang, L. and Liu, H. "Seismic response of clay-pile-raft-superstructure systems subjected to far-field ground motions", *Soil Dynamics and Earthquake Engineering*, **101**, pp. 209–224 (2017).
44. Zhai, P., Zhao, P., Lu, Y., et al. "Seismic fragility analysis of buildings based on double-parameter damage models considering soil-structure interaction", *Advances in Materials Sciences and Engineering*, Article ID 4592847 (2019). https://doi.org/10.1155/2019/4592847
45. Oz, I., Senel, S.M., Palanci, M., et al. "Effect of soil-structure interaction on the seismic response of existing low and mid-rise RC buildings", *Applied Sciences*, **10**(23) (2020). https://doi:10.3390/app10238357
46. Aviram, A., Stojadinovic, B., and Kiureghian, A.D. "Performance and reliability of exposed column base plate connections for steel moment-resisting frames", PEER Report 2010/107, Pacific Earthquake Engineering Research Center (PEER), University of California Berkeley (2010).
47. Zareian, F. and Kanvinde, A. "Effect of column-base flexibility on the seismic response and safety of steel moment-resisting frames", *Earthquake Spectra*, **29**(4), pp. 1537–1559 (2013).

Appendix

τ_{Yi} (yield stress) and G_i (shear modulus) of overlay elements, determined by Kaklamanos [33], are specified here below:

$$\tau_{Y1} = \frac{\tau_2\gamma_1 - \tau_1\gamma_2}{\gamma_1 - \gamma_2}, \tag{A.1}$$

$$\tau_{Yi} = \frac{\tau_{i+1}\gamma_i - \tau_i\gamma_{i+1}}{\gamma_i - \gamma_{i+1}} - \frac{\tau_i\gamma_{i-1} - \tau_{i-1}\gamma_i}{\gamma_{i-1} - \gamma_i},$$
$$i = 2, ..., N-1, \tag{A.2}$$

$$\tau_{YN} = \tau_N - \frac{\tau_N\gamma_{N-1} - \tau_{N-1}\gamma_N}{\gamma_{N-1} - \gamma_N}, \tag{A.3}$$

$$G_1 = \frac{\tau_1}{\gamma_1} - \frac{\tau_1 - \tau_2}{\gamma_1 - \gamma_2}, \tag{A.4}$$

$$G_i = \frac{\tau_{i-1} - \tau_i}{\gamma_{i-1} - \gamma_i} - \frac{\tau_i - \tau_{i+1}}{\gamma_i + \gamma_{i+1}}, \quad i = 2, ..., N-1, \tag{A.5}$$

$$G_N = \frac{\tau_{N-1} - \tau_N}{\gamma_{N-1} - \gamma_N}, \tag{A.6}$$

where $\tau_1, \ldots, \tau_i, \ldots, \tau_N$ are the shear stresses determined according to the chosen shear strains $(\gamma_1, \ldots, \gamma_i, \ldots, \gamma_N)$ and the applied backbone curve.

Biographies

Hadi Sabermahany is a PhD candidate at Civil Engineering Department, University of Tehran, Tehran, Iran. He received his MSc from Sharif University of Technology, Tehran, Iran in 2015. His PhD dissertation

is about numerical investigation of influence of doubly-curved shell raft foundation on seismic response of steel moment-resisting frame buildings considering soil-foundation-structure interaction.

Reza Attarnejad received his PhD degree in 1990 from UPC in Spain focusing on computational mechanics on continuous media. He is currently the (full) Professor at Structural Engineering Division of Civil Engineering Department at University of Tehran. He has extensive publications on his specialties which are fluid-structure interaction, structural dynamics, FEM, applied mathematics, and semi-analytical methods.